The effect of lattice structure on fast electron transport in dual layer solid targets

Contact: nicholas.butler.2014@uni.strath.ac.uk

N. M. H. Butler, R. J. Dance, D. A. Maclellan, R. J. Gray and P. McKenna
Department of Physics, SUPA,
University of Strathclyde, Glasgow, G4 0NG, UK

D. R. Rusby, G. G. Scott, A. P. L. Robinson, D. Neely
Central laser Fasility,
STFC Rutherford Appleton Laboratory,
Oxfordshire, OX11 0QX, UK

M. P. Desjarlais
Sandia National Laboratories,
PO Box 5800, Albuquerque,
NM 87185, USA

B. Zielbauer, V. Bagnoud
PHELIX Group, GSI Hemholtzzentrum
fuer Schwerionenforschung GmbH,
D64291 Darmstadt, Germany

Abstract

The influence of lattice structure and low-temperature electrical resistivity on the transport of fast electrons in solids in investigated numerically using 3D hybrid particle-in-cell (PIC) simulation. Simulations of layered targets, comprised of ordered and disordered carbon allotropes, produce a change in electrical resistivity, without producing a boundary the atomic number.. It is found that the resistive filamentation instability at propagation distances of 60 μm or greater in vitreous material, grows to a level capable of influencing the fast electron propagation. The layer of vitreous carbon is shown to produce filamentation independent of its position in the target provided it is of sufficient thickness (60 μm). This report summarises results that are further detailed in [19] Dance *et al.* in Plasma Physics and Controlled Fusion (at press).

1 Introduction

The transport of large currents (MA) of fast electrons in solid density materials has sustained a high level of research interest over the last two decades due to its wide range of applications such as fast ignition fusion [1, 2], generation of intense x-ray and ion sources [3], and production of warm dense matter (WDM) states with astrophysical relevance [4]. The electrical resistivity of a material is strongly dependent on its lattice structure [9]. Experimental results have highlighted the sensitivity of the transport of fast electrons to the electrical resistivity [7–9]. Intense laser pulses drive electron currents of many mega-Amperes, and these are subject to several instabilities, of which resistive filamentation is more likely to explain the dependency of filamentation on target thickness than instabilities due to ionisation [5, 19]. This filamentation mechanism arises from the growth of self-generated resistive magnetic fields [6].

The growth rate of resistive magnetic fields within the target is described by equation (1) where η is electrical resistivity and j_f is the fast electron current density.

$$\frac{\partial \mathbf{B}}{\partial t} = \eta \nabla \times \mathbf{j}_f + \nabla \eta \times \mathbf{j}_f \quad (1)$$

The self-generated resistive magnetic fields act to pinch the fast electron beam. Small perturbations in the fast electron beam profile develop into localised regions of pinching/hollowing fields around variations in electron density in the beam, and electron filaments are formed.

The duration of a laser-generated fast electron bunch (on ps scale) is short in comparison to lattice melt time (tens of ps) [15–17]. In this case the electrons are quickly heated, and accelerated whilst the ions remain cold.

Figure 1 shows the electrical resistivity (Ωm) as a function of electron temperature (eV). A minimum in resistivity seen at <10 eV in diamond due to the bandgap (5.5 eV). As temperature continues to rise, a transition between electron-phonon scattering to electron-ion collisions occurs, and a minimum in electron mean free path is manifested as a peak in resistivity at ∼50 eV.

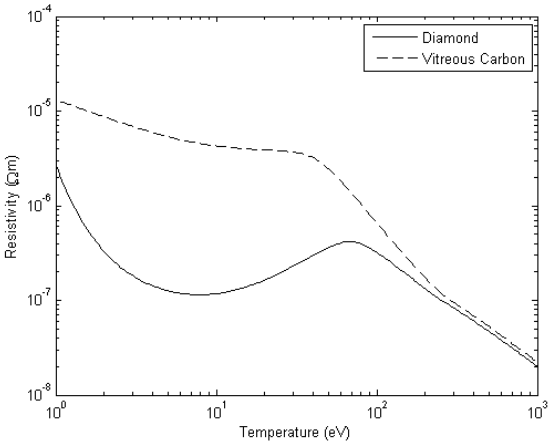

Figure 1: Electrical resistivity as a function of temperature, for the cases of diamond and vitreous carbon

As electrons cross the rear surface boundary, a sheath field that is non uniform is formed and protons acceler-

ated by the TNSA mechanism exhibit a spatial profile mapped from the sheath field strength. The mapping of electron beam structure into sheath field formation allows the fast electron beam transport within the target to be diagnosed by proton spatial intensity profile [10, 11]. The significantly higher resistivity of vitreous carbon (compared to diamond) over the temperature range from a few eV until the onset of the Spitzer regime at ∼80 eV [12], gives rise to an increasingly filamented fast electron beam due to resistive filamentation as discussed in reference [9].

In this brief report, we summarise a numerical investigation of the role of lattice structure in the transport of high currents of fast electrons in layered targets.

2 Simulations

To investigate the underlying electron transport physics, the 3D hybrid-PIC code, Zephyros, [13] was used to simulate the transport of fast electrons within layered carbon targets. In this approach, the fast electron population is described kinetically using the Vlasov equation, which is solved via the PIC method and the background electrons are treated as a fluid. The grid used for all the simulations and is 400 μm × 400 μm × 200 μm, with cell size equal to $\Delta X = \Delta Y = \Delta Z = 1$ μm, and the simulation outputs are sampled at 1.2 ps, just after the bulk of the fast electrons have reached the rear boundary. At this time, any refluxing electrons have had little effect on the main fast electron transport pattern. The laser to fast electron energy conversion efficiency η= 30 %, with a laser pulse duration of 725 fs, wavelength of 1 μm and a focal spot diameter of 2.5 μm. This resulted in a peak intensity of $\sim 1 \times 10^{21} W/cm^2$. The effect of refluxing was minimised by use of 200 μm thick targets. The background temperature is initialised at 1 eV in all simulations, and electrons are injected at [X, Y, Z] = [0, 0, 0], uniformly over a cone with half-angle equal to 40° [18].

To observe the effect of a vitreous material layer preceding an ordered target, a series of simulations were performed where the total target thickness was kept constant $L_T = 200$ μm, and the thickness of the front layer (L_F) of vitreous carbon is varied between L_F=10 μm and 190 μm. The rear surface thickness $L_R = L_T - L_F$ is made up with diamond. Figure 2 shows the results, in which (a)-(e) corresponds to the fast electron density ($\log_{10} m^{-3}$), (f)-(j) is the corresponding resistive magnetic field (T), and (k)-(p) is the corresponding electrical resistivity (Ωm), all in the [Y-Z] mid-plane. In general, as the thickness of the vitreous carbon layer is increased, (going from left to right in figure 2), an increase in filamentation is observed. For cases L_F <50 μm the fast electron transport pattern remains relatively smooth despite the presence of the vitreous layer. For L_F ∼50-60 μm the onset of filamentation can be seen, and for $L_F \gtrsim 60 \mu m$ the beam is strongly filamented. There is little or no evidence of beam transport instabilities within the first 50 μm of the electron source (particularly within the first few tens of microns), as a result of the strong heating within this region. Here, the target is heated well into the Spitzer regime, for which the resistivity decreases with increasing temperature for both vitreous and ordered carbon, as shown in figure 1.

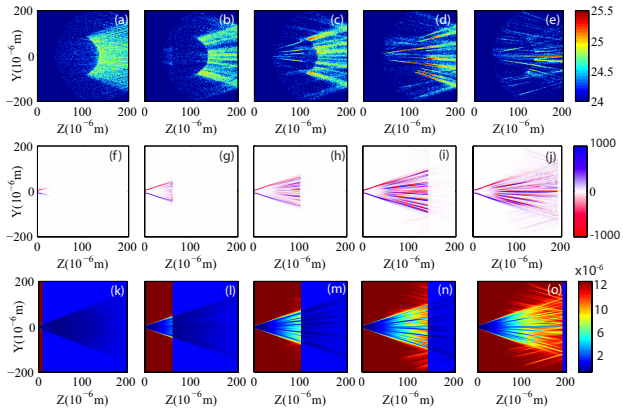

Figure 2: Zephyros simulation results for double layer targets with vitreous carbon as the front layer and diamond as the rear. TOP ROW: Log_{10} fast electron density maps (m^{-3}), in the [Y-Z] mid-plane, for: (a) L_F=10 μm; (b) L_F=50 μm; (c) L_F=100 μm; (d) L_F=140 μm; (e) L_F=190 μm; MIDDLE ROW: Corresponding 2D maps of the magnetic flux density (B_x component in Tesla); BOTTOM ROW: Corresponding 2D maps of electrical resistivity (Ωm).

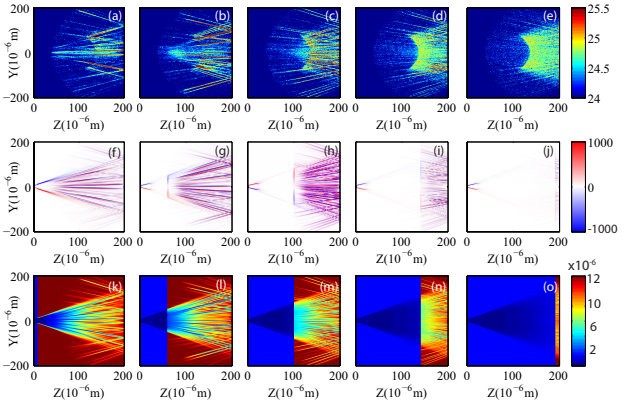

Figure 3: Zephyros simulation results for double layer targets with diamond as the front layer and vitreous carbon as the rear. TOP ROW: Log_{10} fast electron density maps (m^{-3}), in the [Y-Z] mid-plane, for: (a) L_F=10 μm; (b) L_F=50 μm; (c) L_F=100 μm; (d) L_F=140 μm; (e) L_F=190 μm; MIDDLE ROW: Corresponding 2D maps of the magnetic flux density (B_x component in Tesla); BOTTOM ROW: Corresponding 2D maps of electrical resistivity (Ωm).

Equally, to observe the effects of a smooth electron

beam (from an ordered material) impinging onto a vitreous layer, a series of simulations were performed with the order of the layers reversed, i.e. $L_F = 10 - 190$ μm of diamond, with rear surface (L_R) of vitreous carbon and $L_T = 200$ μm. All other conditions remain identical to the previous simulations in figure 2. The results in figure 3 show that as the thickness of the diamond from layer, L_F, is increased a larger density of finer filamentary structure is observed, approaching the limit of a smooth beam (smallest filaments not resolved). The overall fast electron beam pattern is filamented less strongly for L_F >60 μm.

With the vitreous carbon positioned at both the front and rear surface of the target (with diamond on the opposing side), it is seen to produce filamentation in the fast electron beam. The position of the vitreous material appears to play a relatively small role in the degree of filamentation produced, although it does affect the number and size of the filaments.

3 Conclusion

To conclude, our numerical investigation implies that there is a minimum propagation distance of $\sim 60\mu m$ of vitreous material (and implied minimum growth-time), required to allow resistive magnetic fields to evolve to the extent that resistive filamentation of the fast electron beam is observed. In addition, the presence of carbon with disordered lattice structure generates strong filamentary effects, with little dependence on its location within a dual layer target, when its thickness is of the order (or greater) than $60\mu m$.

Acknowledgements

The authors would like to thank the CLF for their continuing support, in particular Dr Alex Robinson for support and use of the Zephyros code. We gratefully acknowledge the use of computing resources provided by STFC's e-Science project. This work is financially supported by EPSRC (grant numbers EP/J003832/1 and EP/K022415/1) and STFC (grant number ST/K502340/1). The research leading to these results is sponsored by the Air Force Office of Scientific Research, Air Force Material Command, USAF, under grant number FA8655-13-1-3008.

References

[1] M. Tabak et al, Phys. Plasmas 1, 1626 (1994)
[2] M. Roth et al, Phys. Rev. Lett. 86, 436-439 (2001)
[3] A. Macchi et al, Rev. Mod. Phys. 85, 751 (2013)
[4] A. Benuzzi-Mounaix et al, Phys. Scr. T161, 014060 (2014)
[5] L. Gremillet, G. Bonnaud, and F. Amiranoff, Phys. Plasmas 9, 941 (2002)
[6] A.R. Bell and R.J. Kingham, Phys. Rev. Lett 91, 035003 (2003)
[7] D. A. Maclellan et al, Phys. Rev. Lett 111, 095001 (2013)
[8] D. A. Maclellan et al, Phys. Rev. Lett 113, 185001 (2014)
[9] P. McKenna et al, Phys. Rev. Lett 106, 185004 (2011)
[10] S. C. Wilks et al, Phys. Plasmas 8, 542-549 (2001)
[11] D.A. Maclellan et al, Laser Part. Beams 31, 475 (2013)
[12] L. Spitzer and R. Harm, Phys. Rev., 89, 5 (1953)
[13] A. P. L. Robinson *et al.*, Phys. Rev. Lett., 108, 125004 (2012)
[14] A. G. R. Thomas *et al.*, J. Comput. Phys., 231, 1051 (2012)
[15] C. W. Siders *et al.*, Science, 12, 286 (2012)
[16] M. D. Kluge *et al.*, J. Chem. Phys. 87, 2336 (1987).
[17] C. V. Shank *et al.*, Phys. Rev. Lett. 50, 454 (1983).
[18] M. Coury *et al.*, Phys. of Plasmas 20, 043104 (2013)
[19] R. Dance *et al.*, Plasma Phys. Cont. Fusion (at press)